Spectroscopy and *ab Initio* Studies of Optical Transitions in Nanostructured ZnO

R. PLUGARU[a], A. DINESCU[a], F. COMANESCU[a], M. PURICA[a],
S. MIHAIU[b], E. VASILE[c], N. PLUGARU[d]

[a]National Institute for Research and Development in Microtechnologies-IMT Bucharest
[b]Institute of Physical Chemistry "I.G. Murgulescu" Romanian Academy
[c]METAV S.A.-CD, Bucharest
[d]National Institute for Materials Physics, Bucharest-Magurele

1.   Introduction

Oxide semiconductors are presently investigated for a wide range of potential device applications, from transistors to optical detection and emission. In this context, zinc oxide (ZnO) is of a particular interest because of its characteristics (wide direct bandgap energy of 3.37 eV and a large binding energy, 60 meV), that makes it one of the best candidates for transparent electronics, sensors and solar cells [1].

A great effort has been brought out to improve the electrical and optical properties of ZnO films, through a diversity of material synthesis techniques, substrates, doping and processing. Electrical conductivity control by Al-doping has received a particular interest, since it may provide a convenient mean for changing the carrier density and mobility [2, 4] combined with useful effects on optical properties in the blue and UV regions of the spectrum [5, 6]. Recently, resistivity values of the order of 10^{-3} - 10^{-4} $\Omega \cdot$cm were reported for Al-doped ZnO thin films with Al concentration between 0.25 and 3.5 at. % [7-10]. For a given Al concentration in the film the resistivity values strongly depend on the method of synthesis and processing, which determine the nanostructure and the defective state. Also, some experiments underscore the fact that increasing Al concentration above approximately 4 at. % has a detrimental effect on conduction and determines an increase in resistivity [8,11]. Still, there is no firm explanation to relate the local structural details in $Zn_{1-x}Al_xO$ to the electrical conduction mechanisms.

On the theoretical side, several comprehensive first principles studies of the electronic structure have attempted to find justifications for the intrinsic n-type

conductivity, the role of defects, as well as the difficulty in achieving p-type conductivity in ZnO (see, e.g., [12-14]). Although there is a conceptual agreement of these studies regarding the role of defects on the electrical and optical properties, one can not yet draw specific conclusions of practical relevance for the control of the conductivity mechanisms. The structure and the way of the dopant impurities incorporated in the films are still under investigation in order to better control the doping process [15-18].

In this contribution, we present results of an investigation on the structure, composition, optical and electrical properties of multilayered ZnO thin films doped with 0.5 at.% Al, prepared by the sol-gel method. The sol–gel process for ZnO and ZnO:Al doped thin films preparation is particularly advantageous because of its simplicity and low cost, composition control, homogeneity on the molecular level. However the crystalline quality of the ZnO prepared by sol–gel process might be inferior to other methods [19]. This effect is caused by the low temperature annealing performed in the sol-gel process that affects the structural and optical characteristics of the thin films. On the other hand, the sol-gel deposition process could present some particularities related to nucleation and growth of nanocrystallites in the thin films formed by multilayers deposition. We bring experimental evidence that when Al^{3+} replaces Zn^{2+} the local structure and the bonding are perturbed so that the defect states favour the electrical and optical conductivity enhancement.

We performed calculations in the Local (Spin) Density Approximation, L(S)DA, of the electronic structure in wurtzite-type ZnO modified by Al doping, aimed at revealing the impurity effects on the conductivity in the disordered matrix. A comparative, first principles study of the electronic structure in wurtzite-type ZnO, modified by M= Al, Ti, Mn doping is also presented, in an attempt to comprehend the impurity effects on conductivity and magnetism in these disordered matrices. Thus, we carried out self consistent calculations on $M_xZn_{1-x}O$ systems (x=0.02, 0.05 and 0.10) using the FPLO release 5.00-20 band structure code. The chemical disorder was treated in the Coherent Potential Approximation, CPA, in the multiscattering formalism of Blackman–Esterling–Berk [20, 21].

2. Experimental

Thin films of Al doped ZnO have been prepared by 1-10 successive layers deposition by sol-gel method on Si/SiO_2 wafers (200 nm SiO_2) and glass substrates (borosilicate glass slides). The starting materials used in the films deposition process were: zinc acetate dihydrate (p.a) $Zn(CH_3COO)_2 \times 2H_2O$ (**ZAD**) (Merck), aluminiumnitrat-nonahydrat $Al(NO_3)3 \times 9H_2O$ (**ANN**), absolute ethanol CH_3CH_2OH (Riedel-deHaen) and triethanolamine $(CH_3CH_2OH)_3N$ (**TEA**) (BAKER ANALYZED). The chart of the deposition process is presented in Figure 1.

Zinc and Aluminium solutions of 0.1 M and 1 M were obtained by dissolving **ZAD** and **ANN** into absolute ethyl alcohol. Zinc acetate solution was stirred up at

60˚C for 15 minutes, then **TEA** was slowly added drop wise in molar ratio of **TEA/ZAD**=1/5 and 1/0.5. The Al-Zn-sol was obtained by adding the appropriate quantity of **ANN** solution to the zinc acetate solution, so that finally represents 0.5% and 5% aluminum atoms in the Al - Zn mixture (ZnO:0.5% at. Al and ZnO:5% at. Al).

The clear and homogenous Al-Zn solution was stored at room temperature for 24 hours before being used for the deposition. After deposition on Si/SiO_2 and glass substrates by dip-coating, each layer was treated at 500^oC for 5 min with a heating rate of 5°C/min for reaching the dwell treatment level.

The thermal treatment was performed in air, by using a Nabertherm type oven. This densification treatment was carried out according to the results of **DTA** and **TG/DTG** analysis presented in Figure 2. **DTA** and **TG/DTG** investigations were performed with a Mettler Derivatograph in the temperature range 20-1000˚C with a heating rate of 5˚C/min.

The thermal analysis of the Al-doped ZnO-dried gel indicates that the total elimination of the organic component occurs at a temperature higher by more than 80˚ than in the case of the zinc acetate (429˚C for the gel and 347˚C for zinc acetate) suggesting the stronger stability of the gel network. The experimental conditions of the films deposition and densification were previously presented in [22]. The coating was repeated 1–10 times. The films were finally annealed at 500^oC for 1 h (post-deposition treatment).

The structural and compozitional characteristics of the films were studied by x-ray diffraction (XRD) (X-ray Diffraction System with triple axis rotating anode-Rigaku SmartLab with Cu Kα radiation) at grazing incidence, transmission electron microscopy (TEM) and high resolution TEM (HRTEM) (TENCAI F30 operated at 300 kV) and energy dispersive x-ray spectroscopy (EDX) in the TEM. The surface morphology was analised by scanning electron microscopy (Field Emission Gun Scanning Electron Microscope (FEG-SEM) - Nova NanoSEM 630) and micro-Raman confocal microscopy (Micro Raman LabRAM HR 800 Horiba). Raman spectroscopy investigation of the successively deposited layers has been performed by using a Micro Raman LabRAM HR 800 Horiba equipment. The Raman spectra, in the 100-1000 cm^{-1} wavenumber range were recorded under laser excitation at 632 nm wavelength and at low incident power (< 5 mW) to avoid sample damage or laser induced heating. The beam diameter was of ~ 1 μm and the laser beam was focused on the sample by a 100 x microscope objective lens. The transmittance and reflectance measurements were carried out by using an UV-Vis-NIR Spectrophotometer-SPECORD M42 equipment, in the wavelength range 200-900 nm. The refractive index and the thickness of the films were determined by spectro ellipsometry method. The ellisopmetric (Ψ, Δ) spectra were recorded with a Spectroscopic ellipsometer SE 800 XUV SENTECH equipment, in the wavelegth range 250-850 nm, with the variable beam diameter (4 to 0.1 mm) and angular variation (0 to 900) with a precision of 0.01^o.

3. Results and Discussion

3.1. *Synthesis of Al doped ZnO multilayered thin films by sol-gel method*

The 1-10 successive layers were deposited by sol-gel method on both Si/SiO_2 wafers and glass substrates. A schematic diagram of the process for Al-doped ZnO multilayered thin films deposition is presented in Figure 1. The thermal treatments were performed using the results of the thermal analysis curves of zinc acetate dihydrate, aluminium nitrate-nonahydrate and Al doped ZnO gel. Thermal analysis provided informations on both the purity of the reagents used as precrusors and on subsequent thermal treatments to be used in order to obtain zinc oxide films doped with aluminum [23].

The thermal effects recorded by DTA up to 1000°C for the zinc acetate dihydrate decomposition and for the prepared ZnO and Al-doped gels are presented in the *Table 1*. For the $Zn\ (CH_3COO)_2\ x\ 2H_2O$ sample the endothermic effect at 92°C indicates the H_2O evolution. The next endothermic effect at 247°C corresponds to the decomposition of acetate. Those two exothermic effects at 322°C and 347°C correspond to the oxidation reaction of the high amount of organics resulted by acetate decomposition, and, probably, crystallization of ZnO.

Table 1. DTA analysis of the Zinc acetate dihydrate and as prepared ZnO and Al-doped gels

Ample	Thermal effects		Assignments
	Endo (°C)	Exo (°C)	
Zn(CH3COO)$_2$ x2H$_2$O	92 247	322 347	Water evolution Acetate decomposition Oxidation of CO to CO_2 Combustion of organic part
Zn-O-gel	76 133 295	311 347 427	Alcohol evolution Water evolution Decomposition of the gel Oxidation of CO to CO_2 Combustion of organic part Crystallization of ZnO
Zn-Al-O gel	79 130 296	429	Alcohol evolution Water evolution Decomposition of the gel Combustion of organic part and crystallization of ZnO

The ZnO and Al-doped ZnO gels present quite similar thermal effects up to 300°C. The first two endothermic effects at 76°C and 133°C, respectively, are assigned to the evolution of ethanol and water. The decomposition of the Zn-hidroxo-acetate gel takes place simultaneously with the oxidation of the resulted CO to CO_2 at about 300°C. The two reactions are accompanied by two small thermal effects, one at 295°C (endothermic peak) assigned to decomposition of the

gel and the other 311°C (exothermic peak) assigned to CO oxidation. The low intensity of the peaks may be explained by the fact that a superposition and a compensation of the two phenomena take place. The exothermic peak at around 387 and 427°C may be assigned to the combustion of organic component and crystallization of ZnO from the studied ZnO gel. In the case of Al-doped ZnO gel appears only one peak at 429°C assigned to the combustion of organic component and crystallization of ZnO. This can be accounted for by the influence of a small amount of nitrate from the aluminium precursor (aluminium nitrate nonahydrate).
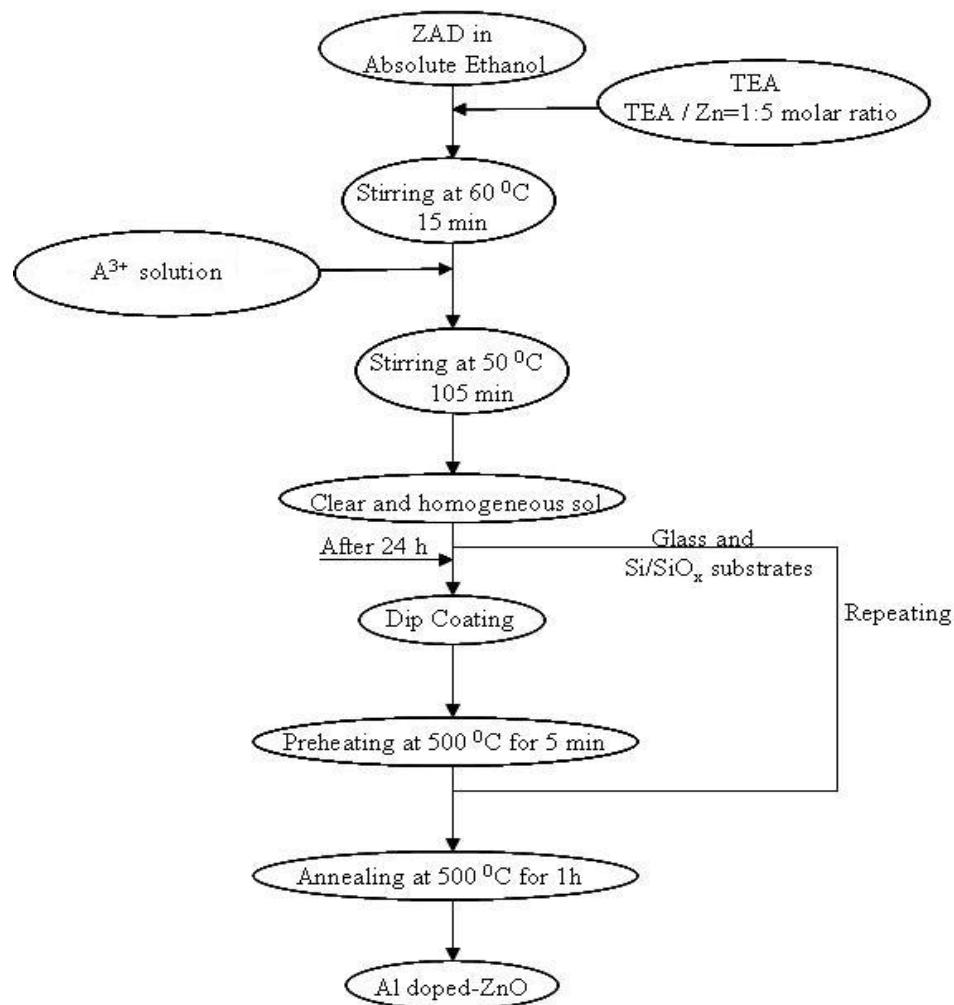
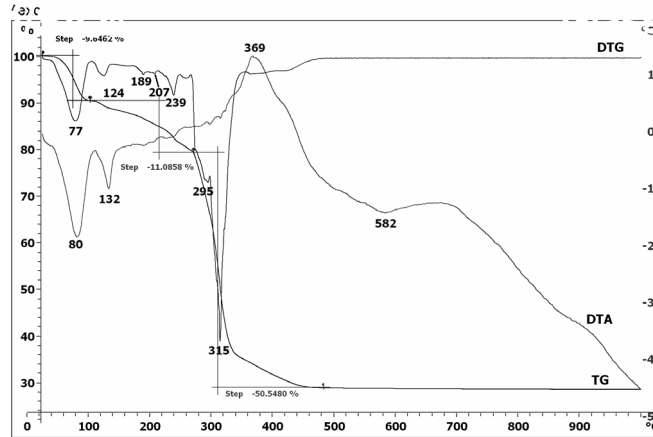**Fig. 1.** Flow chart of Al doped ZnO multilayers deposition by sol-gel method.

Fig. 2. The DTG, DTA and TG evolution of Al doped ZnO gel.

3.2. *Surface morphology*

The SEM images displayed in Figures 3 (a) and (b) show the morphology of the 0.5% Al doped ZnO films formed by 10 layers successively deposited on Si/SiO$_2$ and glass substrates, respectively. In both cases the films present a uniform, compactly packed polycrystalline structure, with the larger grain size between 44.5 and 48.7 nm. A slight unevenness of the films surface may be observed. Regions with a diameter of about 100 nm with smaller grain size occur over the entire surface, suggesting a non-uniform growth process.

The morphology of the films with N=1, 2, 3, 5 and 10 layers successively deposited on Si/SiO$_2$ and glass substrates is shown in Figures 4 (a) and (b).

The SEM images in Fig. 4 (a) and the Raman optical microscopy images presented in Fig.4 (b) demonstrate that the growth process takes place through the nucleation and coalescence of dendritic crystallized areas. All the layers show dendritic structures randomly distributed on their surfaces. The size of the dendritic regions is about 2-4 μm for films with 2 and 3 layers, then, decreases to less than 2 μm for the films with 4 and 10 layers, when films are deposited on a Si/SiO$_2$ substrate (see the sequence of the films from Fig. 4 (a)). Dendritic regions with the size of 1-2 μm for the films with 2 and 3 layers and about 100-200 nm for the films with 4 and 5 layers appear on the surface of the films deposited on glass (see Fig. 4 (b)). In this later case, the film consisting of 10 layers shows a porous structure with pore size of less than 100 nm rather than clusters of separate dendritic structures. Nano-star formation in ZnO: Al (5.0 at. wt.%) thin film deposited by dip-dry method have been reported previously [24].
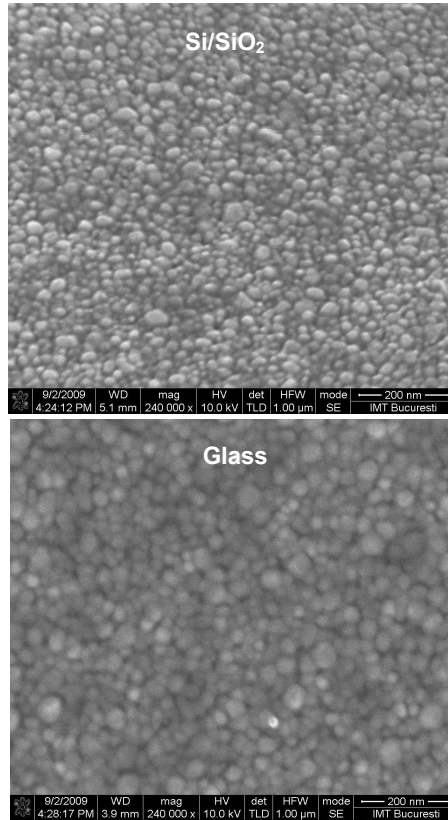
Fig. 3. SEM images of the surface of ZnO:0.5%Al 10 layers films.
grown on Si/SiO$_2$ (a) and glass substrates (b).

The star-shaped structures are considered to be arising from the coalescence of crystallographically oriented ZnO nanoparticles. Doping with Al favors the aggregation of the crystallites and the formation of microstructures. Previous studies have shown that dendrite-like growths of ZnO can be obtained by controlling the aggregated ZnO seeds, [25, 26]. However, for the same nucleation conditions, the morphology of ZnO structures is determined by the rate of aggregation. The anisotropic microstructures with dendritic shape observed in our experiment require a higher growth rate compared with filamentary structures such as the nanowires. Thus, the structure of the films in this work suggests a fast crystallization process. The relatively high temperature, 500°C, used for the consolidation of each deposited layer, can be considered as a dominant factor which controls the agreggation and growth of our polycrystalline films.
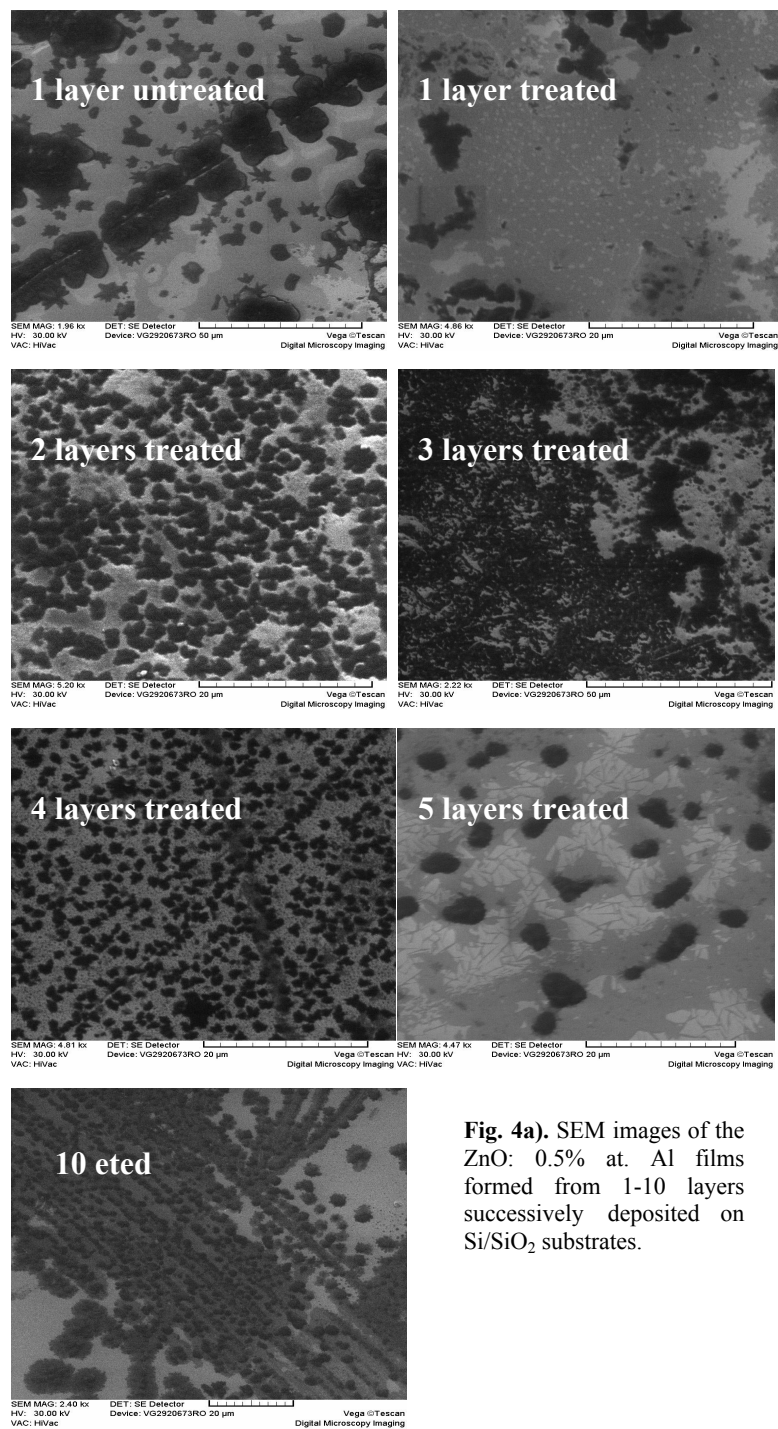
Fig. 4a). SEM images of the ZnO: 0.5% at. Al films formed from 1-10 layers successively deposited on Si/SiO$_2$ substrates.
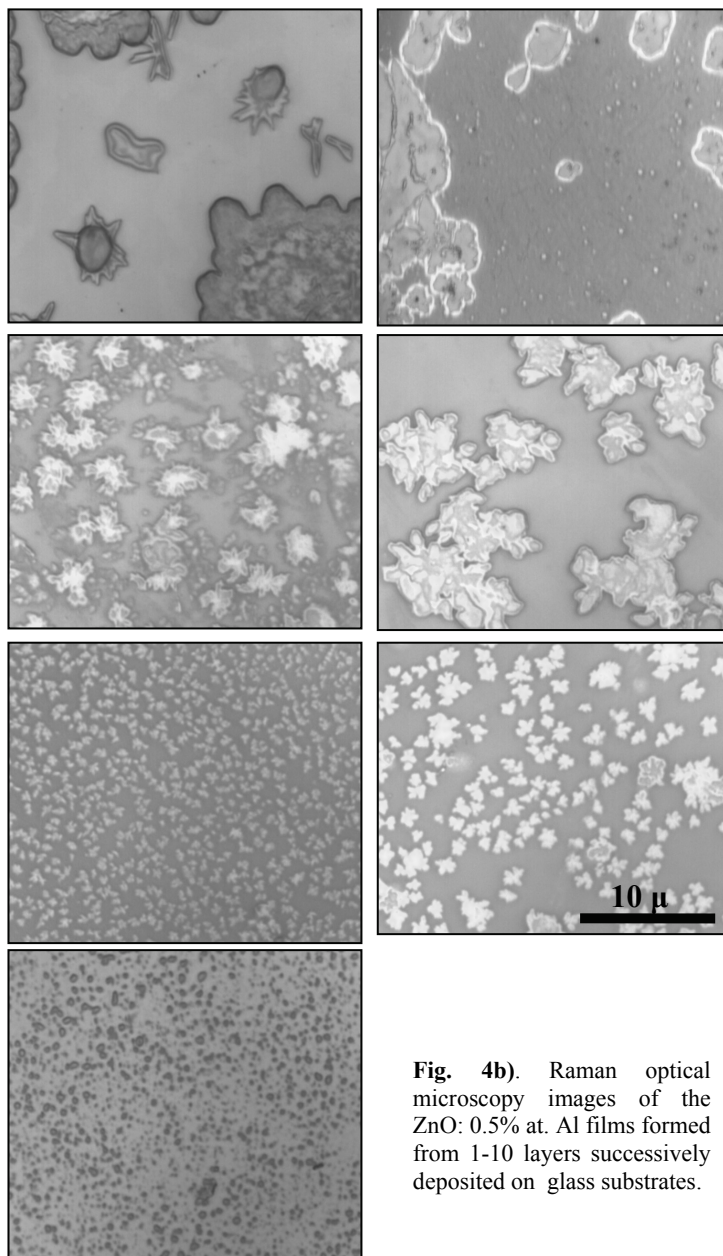
Fig. 4b). Raman optical microscopy images of the ZnO: 0.5% at. Al films formed from 1-10 layers successively deposited on glass substrates.

3.3. *Structural investigation*

The XRD patterns of ZnO:0.5% at. Al doped films consisting of 5 and 10 layers deposited on Si/SiO$_2$ and glass substrates are presented in Figure 5. The patterns

were indexed according to the wurtzite structure (B4). The films grown on Si/SiO_2 are textured, with the c-axis perpendicular to the substrate, as evidenced by the relative intensity of the (002) reflexion. Note that the intensity of the (002) line increases with the number of deposited layers, clearly pointing to a texture induced by the film growth process. In case the films grow on glass substrate, the orientation gradually changes from (002) to (101) after 5 layers deposition.
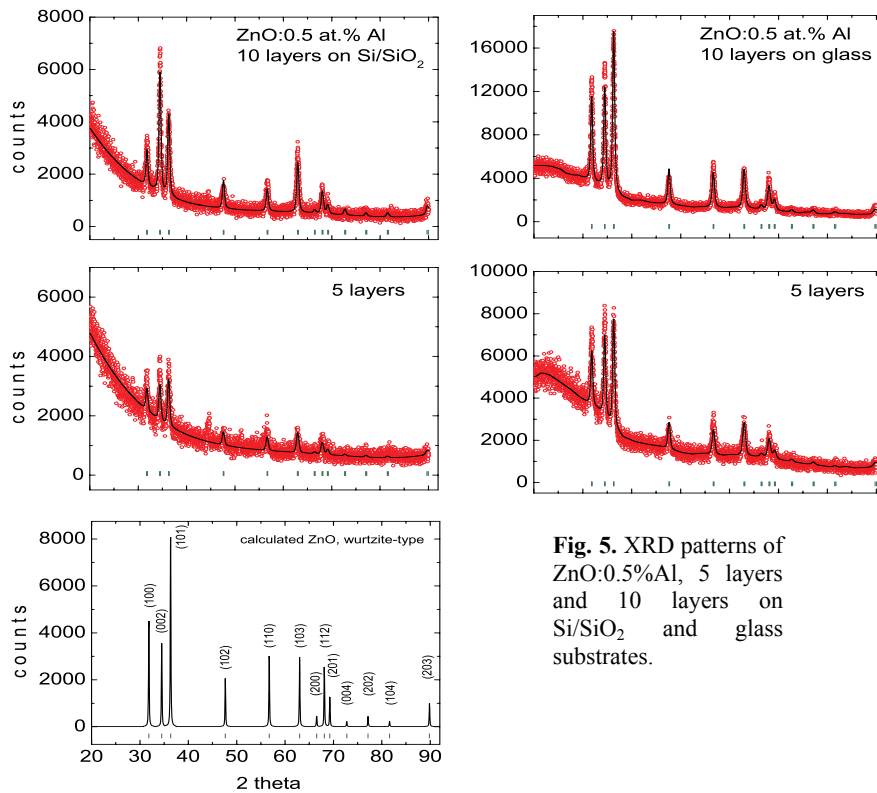

Fig. 5. XRD patterns of ZnO:0.5%Al, 5 layers and 10 layers on Si/SiO_2 and glass substrates.

Figure 6 and Figure 7 display the TEM images and the corresponding selected area diffraction (SAED) of the films with 10 layers deposited on Si/SiO_2 and glass substrates. The films consist of crystalline grains embedded in an amorphous matrix. The HRTEM image presented in the inset in Fig. 6 reveals the lattice fringes of nanocrystals inside a grain in the film deposited on Si/SiO_2 substrate. The interplanar distances of 2.84 Å and 2.45 Å, corresponding to the planes (100) and (101) in ZnO wurtzite structure are indicated. Thus, the micrographs support a (002) texture perpendicular to the film plane, in accordance with the XRD results.

An inspection of the HRTEM image of the film grown on glass (see Fig.7), shows that the lattice fringe is about 2.48 Å and 1.92 Å which corresponds to the

(101) and (102) planes; therefore, the preferred growth direction is along the [100] axis for the films deposited on glass [27, 28].

   The diameter of the nanocrystallites in a grain varies in the range 2-15 nm for the films deposited on silicon substrate (Fig. 6), and 6-10 nm in the case of the films deposited on glass substrate (Fig. 7). The HRTEM images also show that the crystallization of a grain in the film deposited on Si/SiO_2 is better than in the case of the film deposited on glass. Not only the size of the crystallites, but also their density in a grain is higher in the former case.
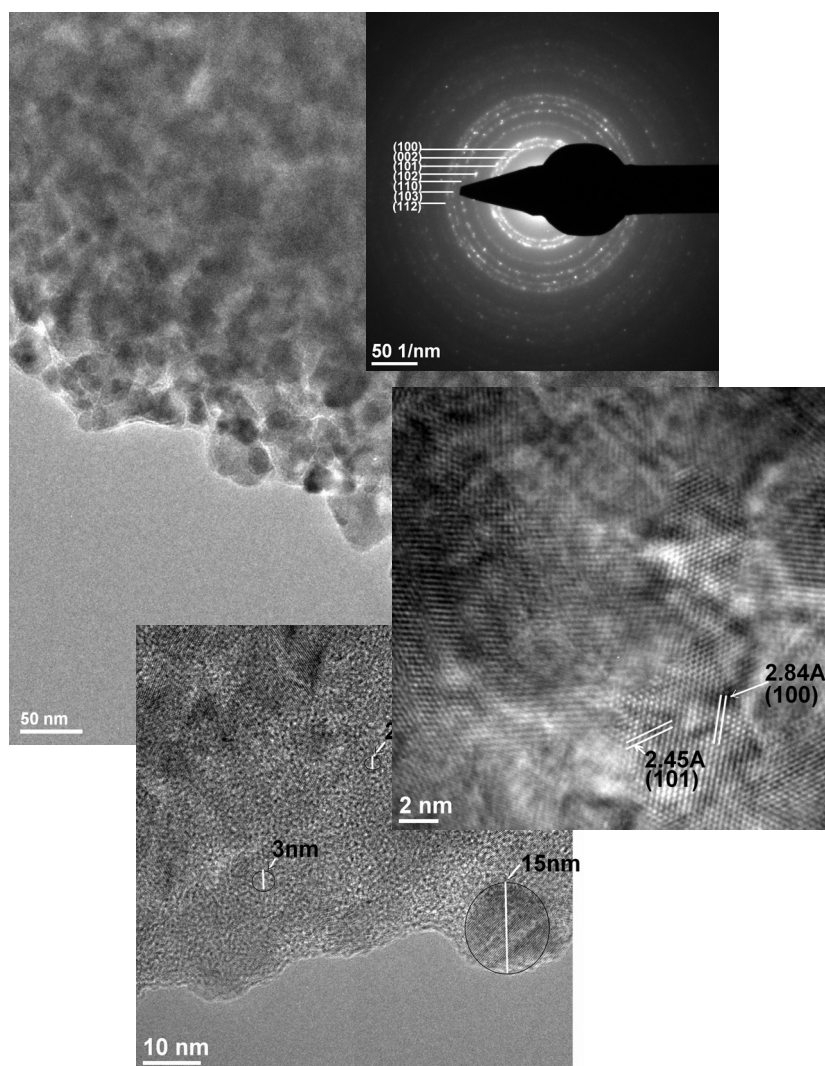

Fig. 6. TEM images and the corresponding selected area diffraction (SAED) of the films with 10 layers deposited on Si/SiO_2.
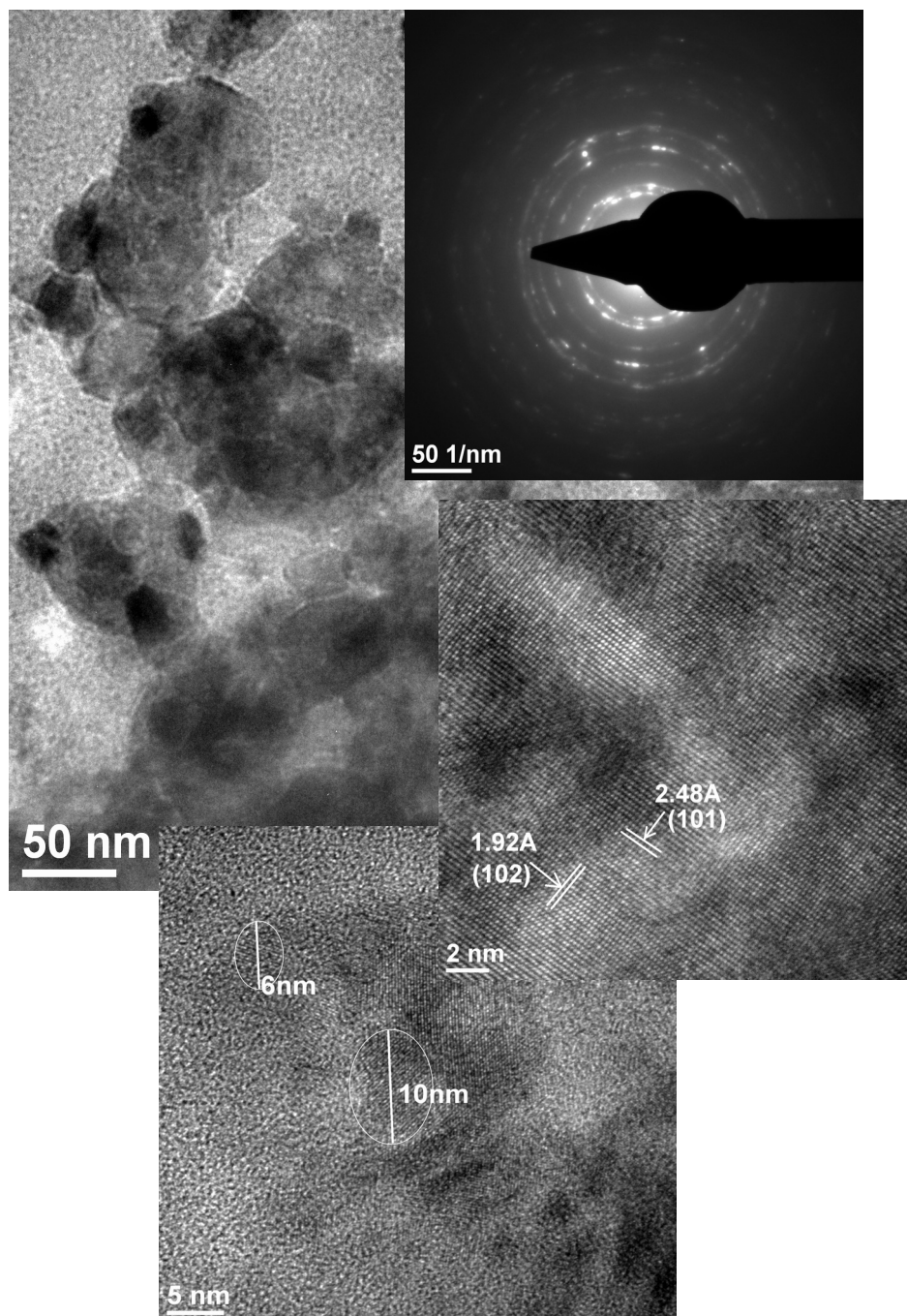
Fig.7. TEM images and the corresponding selected area diffraction
(SAED) of the films with 10 layers deposited on glass.

EDX analysis was performed to study the elemental composition of the ZnO:0.5% at. Al doped films. The average concentration of Al in the films is 0.40 ±0.10 at. %. The concentration of the elements in a selected area of the film with 5 layers deposited on a Si/SiO$_2$ substrate is presented in *Table 2*. The EDS spectra corresponding to qualitative and quantitative analysis are showed in Figures 8 (a) and (b). The film with 10 layers demonstrates a concentration of 0.57 at.% in a plan view selected area, while in a cross section area corresponding to a nanocrystalline grain (see Figure 9), Al concentration is 0.13 at.%.

Table 2. Concentration of Al in the ZnO:0.5% at. Al with 5 layers

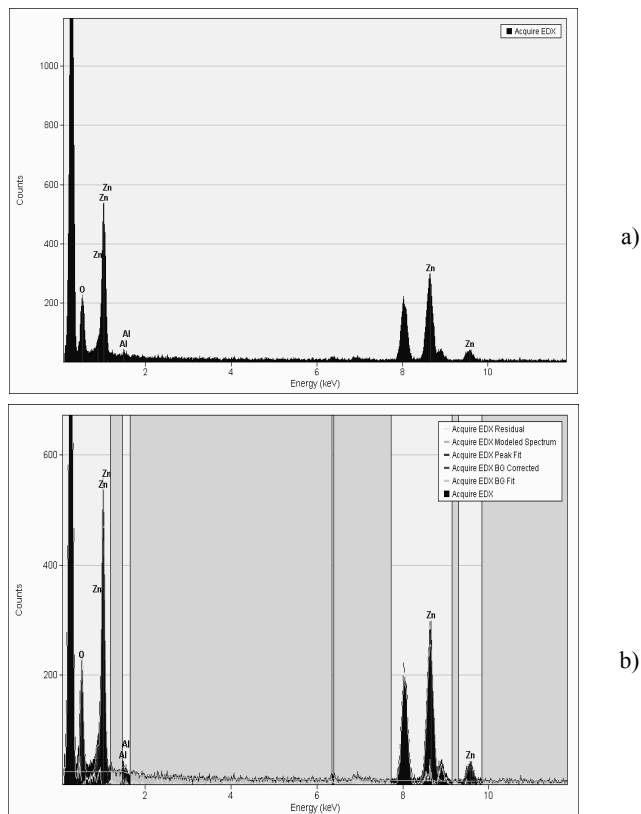| Element	Weight %	Atomic %	Uncert. %	Correction	k-Factor
--------	--------	--------	--------	--------	--------
O(K)	32.76	66.41	0.76	0.49	2.008
Al(K)	0.31	**0.37**	0.08	0.92	1.030
Zn(K)	66.92	33.20	0.92	0.99	1.68

Fig. 8. Energy dispersive spectra (EDS) spectra of ZnO:0.5% at. Al film with Cantitative microanalyse (view of quantization spectrum). 5 layers. (a) Calitative microanalyse; (b).
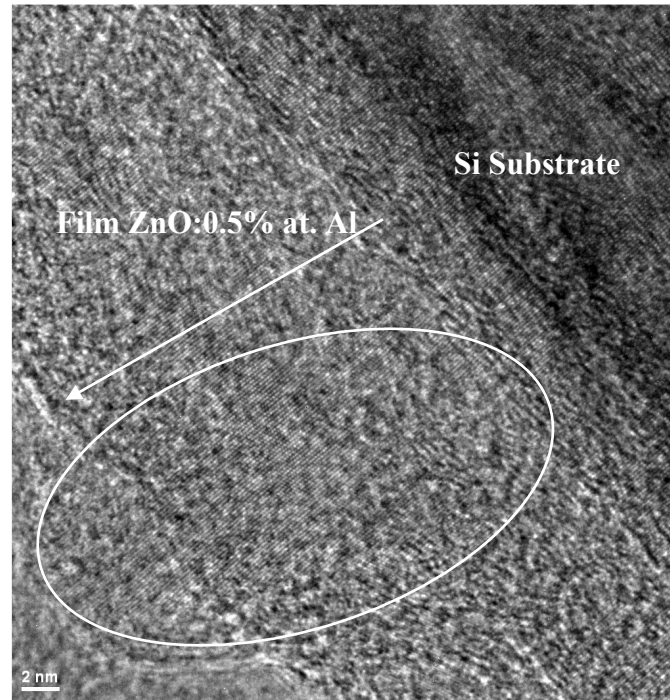
Fig. 9. HRTEM cross section image of the film ZnO:0.5% at. Al, formed from 10 layers.
The nanocrystalline grain in the film is pointed out.

3.4. *Optical investigation*

The optical transmission and absorption spectra of the films doped with 0.5 %
at. Al and 5 % at. Al, recorded in the wavelength region 200-900 nm are plotted in
Figures 10 (a) and (b). The optical transmission spectra of the undoped films with 1
layer and 4 layers are included for comparison (Fig. 10 (a)). It can be observed that
the optical transmittance of the films varies in the range of 80%-95%. The
transmittance decreases when it's increased the number of the layers in the case of
the 0.5% at. Al doping, but it remains almost constant for 5% at.Al doping as well
as for the undoped films. For the same number of deposited layers, the
transmittance decreases when Al concentration increases. The present result is in
conceptual agreement with previously reported data [28] on the transmittance of
multilayer films doped with Al in the range 0.25 % to 4 %. The optical absorption
spectra of the films are shown in Figure 10 (b). The optical band edge of ZnO: Al
doped films calculated from transmission spectra are shifted comparatively to the
value 3.92 eV obtained for undoped films. The values of 3.76 eV and 4.12 eV were
calculated for 0.5 % at. Al and 5 % at. Al doped films, respectively. The shift of the
absorption band edge to higher energies in Al doped ZnO films was observed for

Al concentration up to 3 at. % [29]. The optical band gap value (E_{opt}) increases from 3.27 eV up to 3.33 eV, then decreases to 3.28 eV [30]. Also, enhanced E_{opt} values of 3.70-3.87 eV were reported for 5 mol% and 8 mol% Al doped films prepared by sol-gel method, whereas the E_{opt} of the undoped films was 3.70 eV [31]. The higher values of E_{opt} for undoped and doped films obtained in our experiment comparatively to previously reported results can be related to structural differences, particularly to the porosity observed in our films, which affects the optical constant.
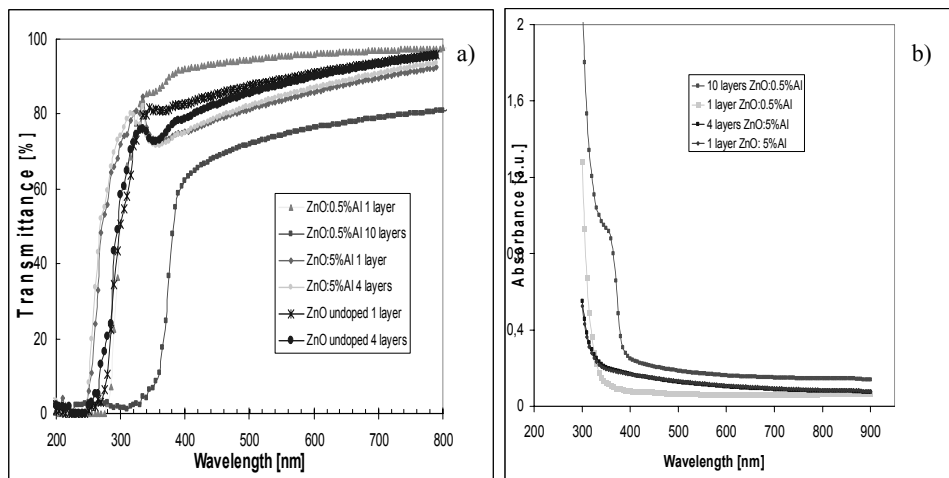

Fig. 10. Optical transmission (a) and absorbtion (b) spectra of ZnO, ZnO: 0.5% at. Al and ZnO: 5% at. Al doped multilayers films.

The films refractive index, $n(\lambda)$, and the thickness were determined from spectroscopic ellipsometry measurements of optical constants in the wavelength range 250-850 nm. Figure 11 shows $n(\lambda)$ for 1, 4, 10 layers of 0.5 % Al: ZnO. For all the samples the refractive index values are lower, n =1.6-2, comparatively with the refractive index of an epitaxial ZnO layer in the visible region (n = 1.9-2.1) [32]. This difference can be attributed to a lower density of our films.

The dependence of the film thickness versus the number of depositions for ZnO:5 % Al is shown in the plot in Fig. 12. The curve shows a slight deviation from a linear dependence for up to 5 depositions and then deviates stronger for 5 to 10 depositions. The same trend is also observed for the 0.5 % Al concentration, but with a lower rate of the layer deposition. We obtained a thickness of 31 nm per deposited layer for 5 % Al and only 16 nm per layer for 0.5% Al concentration. Comparatively, the thickness of an undoped layer was 8 nm. The dependence of the observed deposition rate on the dopant concentration shows that the Al ions act as nucleation centers.
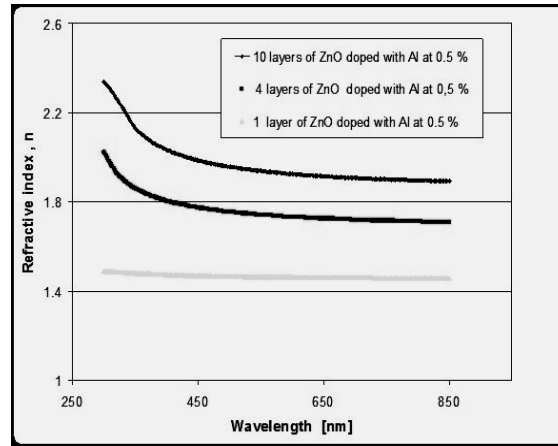
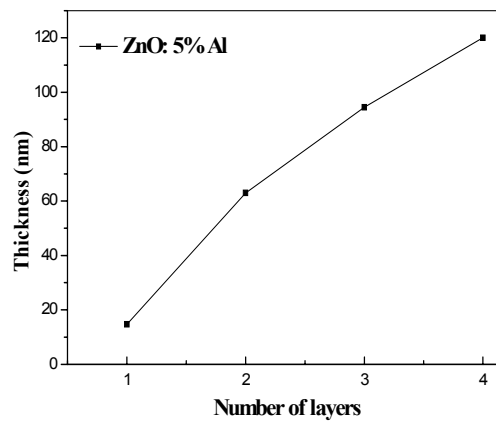**Fig. 11.** Refractive index of N=1, 4, 10 layers ZnO:0.5% at. Al films.

Fig. 12. Film thickness versus the number of
depositions for ZnO:5% Al doped films.

3.5. *Raman spectroscopy*

Fig. 13 shows the Raman spectra of the ZnO:0.5 % Al films with 4 and 10 layers deposited on Si/SiO2 substrate. For comparison, the Raman spectrum of ZnO micro-rods grown by CVD is included in the same figure. The wurtzite structure belongs to space group C6v and, according to group theory, the optical phonons at the Γ point of the Brillouin zone are A1+2B1+E1+2E2 [34]. The A1, E1, 2E2 modes are Raman active while 2B1 are silent. The polar phonons of A1, E1 modes are split into longitudinal optical (LO) and transversal optical (TO) components - A1 (TO), A1 (LO), E1 (TO), E1 (LO). Non-polar phonon modes, E2, have two frequencies: E2 (low) associated with non-polar vibration of the heavier Zn atoms sublattice and E2 (high) mode with lighter oxygen atoms. The Raman

spectra were recorded with the laser beam focalized on the dendritic structures, covering an area with a diameter of about 1 μm. The peak located at 437 cm^{-1} in the spectra of the ZnO:0.5% at. Al films can be assigned to the E2 (high) mode of non-polar optical phonons. This is the characteristic peak of hexagonal wurtzite phase and for the bulk ZnO is situated at 439 cm^{-1}. The Raman peak corresponding to E2 (high) mode in the spectra of the ZnO nanocrystals is redshifted compared with bulk material. The redshift effect has been previously attributed to the relaxation of the selection rules in the case of small particles, such as nanocrystallites with 20 nm size, or due to the doping effect [35]. In the latter case, one may also expect a broadening of the Raman peak. The local heating produced by the laser has also been considered to be at the origin of the red shift [36].
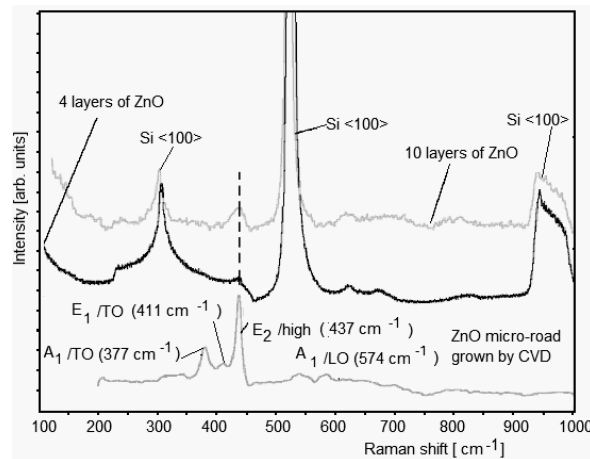

Fig. 13. Ran spectra of 0.5% Al:ZnO films with 4 and 10 layers. For comparison, the Raman spectrum of ZnO micro-rods grown by CVD [ref 26] is also presented.

In the Raman spectra plotted in Fig. 13, the peak associated with the E2 (high) mode appears red shifted for all the samples. However, the broadening effect can be observed only for the peaks in the spectra of the sol-gel deposited films and it is likely to be caused by dopant impurities. No other modes are visible in the spectra of the films, most likely due to the presence of free carriers in the samples or due to the hidden effect caused by the high intensity of the Raman peaks from the Si substrate. The increase in the peak intensity of the E2 (high) mode with the number of the deposited layers confirms the nanocrystallinity of the films deposited layer by layer.

3.6. *UV-VIS Fluorescence*

The fluorescence spectra of the films obtained by deposition of 1-10 layers on Si/SiO$_2$ and glass substrates are shown in Figure 14 (a) and (b). Two emission bands are present in the spectra, one situated at 383 nm (3.23 eV) and the other

situated in the blue region at 400-450 nm (3.1-2.75 eV). Comparatively, the fluorescence spectra of undoped films (not shown here) are dominated by the optical transitions at 386 nm (3.21 eV) in the case of the films grown on Si/SiO$_2$ and 387 nm (3.20 eV) in the case of the films grown on glass. A blue shift is observed in the fluorescence emission spectra of the doped films. The optical band gap shift towards the shorter wavelength can be ascribed to Burstein-Moss effect [37]. The increase in carrier concentration in the doped films leads to the occupation of the conduction band bottom, then, the lowest states in the conduction band are forbidden for the occurrence of optical transitions. Previously, it was reported that the optical band gap in ZnO shifts from 3.40 eV to 3.55 eV, for a doping concentration of 0.95% at Al, [37]. In our case the blue shift is smaller, in consistency with the smaller Al concentration in our films. It is worth to observe the intense blue emission bands in the plots in Fig.14. We suggest that these bands correspond to transitions involving defect levels induced by Al doping [38-41].
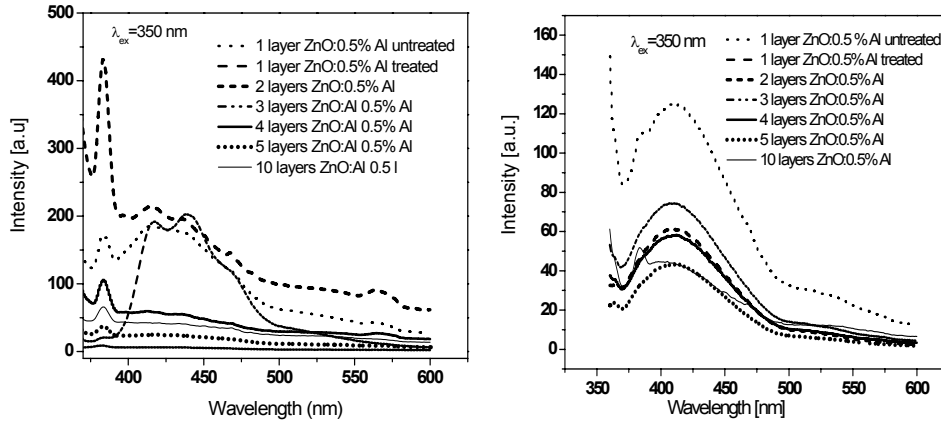

Fig. 14. Fluorescence spectra of ZnO: 0.5% at. Al multilayer films on Si/SiO$_2$ (a) and glass substrates (b) at an excitation wavelength of 350 nm.

3.7. *DFT study of the electronic structure of*
$M_x Zn_{1-x} O$ *(M=Al, Ti, Mn)*

We performed calculations of the electronic band structure of wurtzite-type ZnO modified by M=Al, Ti and Mn doping, aimed at disentangling the impurity effects on conductivity and magnetism in these disordered matrices [42, 43]. We used the exchange and correlations functional in the parameterization of Perdew and Wang [44] and a 16×16×16 integration grid in the Brillouin zone to account for possible Fermi surface effects, having in view the donor character of Al and Ti. We performed the calculations at the experimental volume, assumed the impurity substitutional character and considered no lattice relaxation, hence we refer only to the electronic effects due to the substitutions.

Al and Ti substitution for Zn leads to the appearance of donor states in the system. The valence band shifts to lower energy and a density of states, $N(E_F)$, arises at the Fermi level, increasing with the dopant concentration. The evolution of the band structure as a result of Al and Ti doping may be observed in the element and angular momentum-projected DOS plots displayed in Figure 15 and Figure 16, respectively. The present results indicate that Al-doped ZnO is already metallic for $x = 2\%$. The Al 3s and 4s states are partially occupied and form a narrow band localized at the valence band minimum, see Figure 15. Al contribution to $N(E_F)$ at the Fermi level is almost negligible for 2 at.% Al. Therefore, we associate the conductivity increase in Al-doped ZnO films mostly with the presence at the Fermi level of the electronic charge from O 2p dangling orbitals.
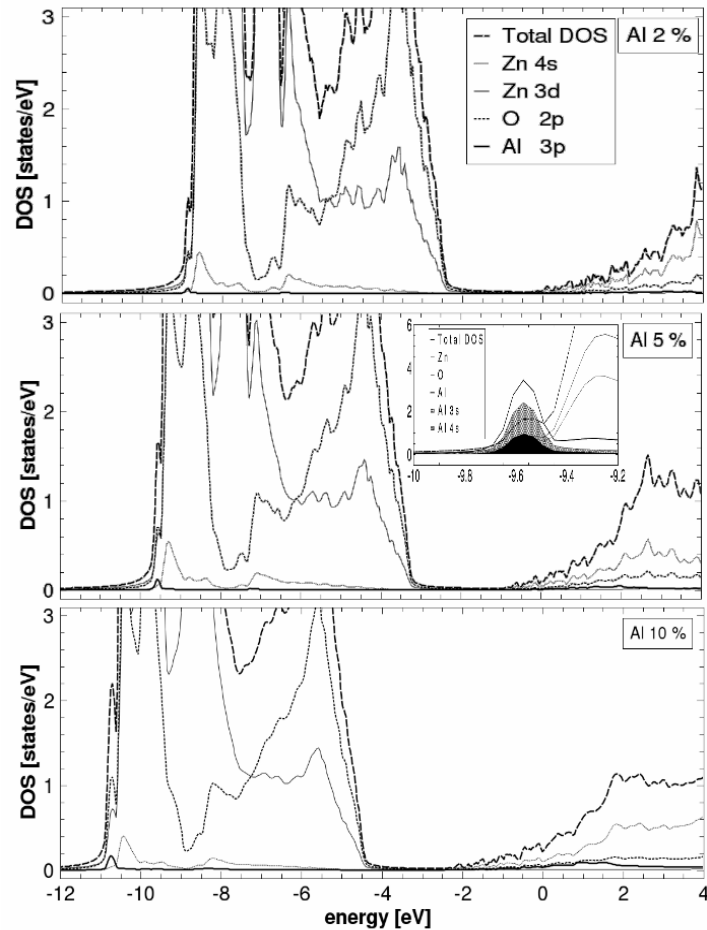

Fig. 15. Tott and l-projected DOS of ZnO doped with: i) 2 % Al top panel, ii) 5 % Al middle panel and iii) 10 % Al bottom panel. Inset middle panel: Enlarged image of the valence band bottom showing Al 3s and 4s states. Note that the Al states are scaled.
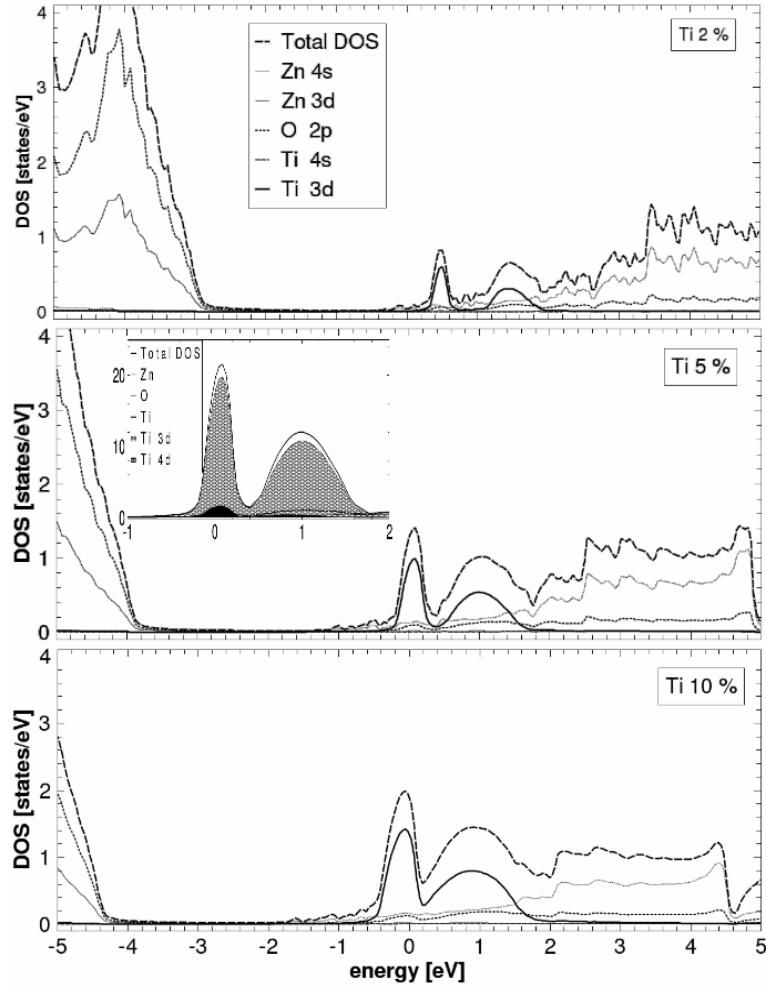
Fig. 16. LDA total DOS and element and l-projected DOS of ZnO doped with: i) 2 % Ti,
top panel, ii) 5 % Ti, middle panel and iii) 10 % Ti, bottom panel. Inset middle panel:
Enlarged image of the region at the Fermi energy showing the contribution of
Ti 3d and 4d states at the N(E$_F$).

   The LDA results for Ti doping show a peak in the density of states at the Fermi level, due to Ti(3d) states, mainly, and also Ti(4d) states, secondarily, see Fig. 5; these states also contribute to a peak situated at approx. 1 eV in the CB, see Inset in Figure 16. N(E$_F$) shows a variation determined by the shift of the Fermi level toward the CB; thus, N(E$_F$) increases uniformly from 0.04 states/eV for 2% Ti, to 1.93 states/eV for 10% Ti. Our results predict a non magnetic ground state for Al doped ZnO, derived from a comparison of total energy in spin unpolarized and spin

polarized calculations, in consistency with reported results. In the case of Ti doping the impurity band at the Fermi level is exchange split and the calculations predict a magnetic ground state, in agreement with previous experimental [45] and first principles [46] results. Previously, it has been established that carrier mediated ferromagnetism is responsible for the magnetism in diluted magnetic semiconductors (DMS) [47].

The Mn-doped system retains its semiconductor character for x up to 10%; at that concentration it is at the limit of undergoing an insulator-to-metal transition. The Mn majority spin t_{2g} and e_g states (fully occupied) are situated in the band gap, whereas the (unoccupied) minority spin states are in the conduction band. In the case of Ti doping the LSDA magnetic moment increases from 0.90 to 1.13 to 1.28 μ_B/Ti at. for x=2%, 5% and 10%, respectively, pointing to Ti^{2+} configuration, whereas in the case of Mn the magnetic moment is constant, 4.71 μ_B/Mn at. (high spin Mn^{2+} configuration) in the 2-10% concentration range.

4. Conclusions

- Al-doped ZnO multilayered films (N $\leq$ 10 and Al concentration 0.5 and 5 %) with wurtzite structure were grown by sol-gel route on Si/SiO_2 and glass substrates.
- The films are polycrystalline with the grain size of about 44.5-48.7 nm on both types of substrates. The growth process takes place by the nucleation of dendritic structures which coalesce; this process leads to grains with a certain degree of porosity.
- The transmittance of the 1-10 layers of Al:ZnO is 80-95% and decreases when increasing the number of layers. The optical band edge of ZnO is shifted to a shorter wavelength (blue shift) when Al concentration increases. The thickness of a layer increases with Al concentration, from 8 nm for the undoped film, to 16 nm for 0.5% Al and to 31 nm for 5 % Al.
- The E2 (high) Raman mode shows 2 cm^{-1} red shift and appears as a broad peak in the Raman spectra of the multilayered films. The peak intensity of the E2 (high) mode increases with the number of the deposited layers; therefore it brings evidence on the nanocrystallinity of the films deposited layer by layer.
- Fluorescence emission of the films doped with 0.5% at. Al shows the presence of defects, interstitial Zn, and oxygen vacancies (OVs) with the associated emission bands. We assigned the observed blue emission in the region 400-450 nm to transitions involving defect levels induced by the Al substitution for Zn.
- A shift of the fluorescence band at 383 nm to ultra-violet region is determined for Al concentration of 0.4 ±0.1 % with respect to the undoped ZnO. The optical band edge of ZnO is shifted to a shorter wavelength

       when increasing Al concentration (blue shift) according with the Moss–Burstein theory.

- Ab-initio calculations predict that in wurtzite-type ZnO systems modified by M= Al, Ti and Mn: i) Al, Ti, Mn behave as donors; ii) Al, Ti, Mn demonstrate different effects on conductivity and magnetism; iii) local magnetic moments appear in Ti and Mn doped ZnO.

References

[1] DJURIŠIĆ A.B., NG A.M.C., Chen X.Y., *ZnO nanostructures for optoelectronics: Material properties and device applications*, Progress in Quantm Electronics **34**, pp. 191–159, 2010.

[2] JANOTTI A. and WALLE VAN de C.G., *Fundamentals of zinc oxide as a semiconductor*, Rep. Progr. Phys. **72**, 126501(29), 2009.

[3] JAGADISH C. and PEARTON S., (Editors), *Zinc Oxide Bulk, Thin Films and Nanostructures*, Elsevier, 2006.

[4] SAGAR P., KUMAR M., MEHRA R.M., *The Meyer–Neldel rule in sol–gel derived, polycrystalline ZnO:Al thin films*, Solid State Commun, **147**, pp. 465–469, 2008.

[5] DING J.J., MA S.Y., CHEN H.X., SHI X.F., ZHOU T.T., MAO L.M., I*nfluence of Al-doping on the structure and optical properties of ZnO films*, Physica B **404**, pp. 2439–2443, 2009.

[6] ELILARASSI R., CHANDRASEKARAN G., *Effect of annealing on structural and optical properties of zinc oxide films*, Mater. Chem. Phys. **121**,pp. 378–384, 2010.

[7] LIN -moh K., CHEN Y.-Y., CHOU K.-Y., *Solution derived Al-doped zinc oxide films: doping effect, microstructure and electrical property*, J. Sol-Gel Sci. Technol. **49**, pp. 238–242, 2009.

[8] LU J.J., TSAI S.Y., LU Y.M., LIN T.C., GAN K.J., *Al-doping effect on structural, transport and optical properties of ZnO films by simultaneous RF and Dc magnetron sputtering*, Solid State Commun. **149**, pp. 21777–2180, 2009.

[9] QIANG X.Z., HONG D., YAN L., HANG C., *Al-doping effects on structure, electrical and optical properties of c-axis-orientated ZnO: Al thin films*, Mat. Sci. Semicon. Processing **9**, pp. 132–135, 2006.

[10] ZHU M.W., GONG J., SUN C., XIA J.H., JIANG X., *Investigtion of correlation between the microstructure and electrical properties of sol-gel derived ZnO based thin films*, J. Appl. Phys. **104**, pp. 073113–7, 2008.

[11] LUPAN O., CHOW L., SHISHIYANU S., MONAICO E., SHISHIYANU T., SONTEA V., ROLDAN CUENYA B., NAITABDI A., PARK S. and SCHULTE A., *Nanostructured zinc oxide films synthesized by successive chemical solution deposition for gas sensor applications*, Mat. Res. Bulletin **44**, pp. 63–69, 2009.

[12] WALLE Van de C.G., *Computational studies of conductivity in wide-band-gap semiconductors and oxides*, J. Phys.: Condens. Matter **20**, pp. 064230–7, 2008.

[13] IUSAN D., KNUT R., SANYAL B., KARIS O., ERIKSSON O., COLEMAN V.A., WESTIN G., MAGNUS J., SVEDLINDH P., *Electronic structure and chemical and magnetic interactions in ZnO doped with Co and Al: Experiments and ab-initio density-functional calculations*, Phys. Rev.B **78**, pp. 085319-1–9, 2008.

[14] PALACIOS P., SANCHEZ K., WAHNON P., *Ab-initio valence band spectra of Al, In doped ZnO*, Thin Solid Films **517**, pp. 2448–2451, 2008.

[15]   SHELKE V., SONAWANE B.K., BHOLE M.P., PATIL D.S., *Effect of annealing temperature on the optical and electrical properties of aluminum doped ZnO films*, J. Non-Cryst. Solids **355**, pp. 840–843, 2009.

[16]   MALDONADO F., STASHANS A., *Al-doped ZnO: Electronic, electrical and structural properties*, J. Phys. Chem. Solids **71**, pp. 784–787, 2010.

[17]   EHRMANN N., REINEKE-KOCH R., *Ellipsometric studies on ZnO: Al thin films: Refinement of dispersion theories*, Thin Solid Films **519**, pp. 1475–1485, 2010.

[18]   CHUAN YAO P., TSE HANG S., SHUAN LIN Y., TSAI YEN W., CHENG LIN Y., *Optical and electrical characteristics of Al-doped ZnO thin films prepared by aqueous phase deposition*, App. Surf. Sci. **257**, pp. 1441–1448, 2010.

[19]   ZNAIDI L., *Sol–gel-deposited ZnO thin films: A review*, Mat. Sci. Eng. B **174**, pp. 18–30, 2010.

[20]   KOEPERNIK K. and ESCHRIG H., *Full-potential nonorthogonal local-orbital minimum-basis band-structure scheme*, Phys. Rev. B **59**, pp. 1743–1757, 1999.

[21]   KOEPERNIK K., VELICKÝ B., HAYN R. and ESCHRIG H., *Self-consistent LCAO-CPA method for disordered alloys*, Phys. Rev. B **55**, pp. 5717–5729, 1997.

[22]   MIHAIU S., GARTNER M., VOICESCU M., GABOR M., MOCIOIU O., ZAHARESCU M., *Characterization of the ZnO thin films obtained by chemical route*, Optoelectron. Adv. Mater. Rapid Communications **3**, pp. 884–890, 2009.

[23]   MIHAIU S., TOADER A., ATKINSON I., ANASTASESCU M., VASILESCU M., ZAHARESCU M., PLUGARU R., *Al–doped ZnO nanocoatings obtained by sol-gel route*, Proceedings of SPIE Advanced Topics in Optoelectronics, Microelectronics, and Nanotechnologies V, **7821**, pp. 7821–70, 2010.

[24]   BEHERA D., ACHARYA B.S., *Nano-star formation in Al-doped ZnO thin film deposited by dip-dry method and its characterization using atomic force microscopy*, electron probe microscopy, photoluminescence and laser Raman spectroscopy, J. Luminescence **128**, pp. 1577–1586, 2008.

[25]   ZHANG H., DU N., WU J., MA X., YANG D., ZHANG X., YANG Z., *A novel low-temperature chemical solution route for straight and dendrite-like ZnO nanostructures*, Mater. Sci. Eng. B **141**, pp. 76–81, 2007.

[26]   XIE J., LI P., WANG Y., WEI Y., *Synthesis of needle- and flower-like ZnO microstructures by a simple aqueous solution route*, J. Phys. Chem. Solids **70**, pp. 112–116, 2009.

[27]   KIM S., KANG H.-G., CHOI J., *Surfactant-free preparation of ZnO dendritic structures by electrochemical method*, Current App. Phys. **10**, pp. 740–743, 2010.

[28]   HUANG J., XIA C., CAO L., ZENG X., *Facile microwave hydrothermal synthesis of zinc oxide one-dimensional nanostructure with three-dimensional morphology*, Mat. Sci. Eng. B **150**, pp. 187–193, 2008.

[29]   LIN -moh K., CHEN Y.-Y., CHOU K.-Y., *Solution derived Al-doped zinc oxide films: doping effect, microstructure and electrical property*, J. Sol-Gel Sci. Technol. **49**, pp. 238–242, 2009.

[30]   DING J.J., MA S.Y., CHEN H.X., CHEN X.F., SHI X.F., ZHOU T.T., MAO L.M., *Influence of Al-doping on the structure and optical properties of ZnO films*, Physica B **404**, pp. 2439–2443, 2009.

[31]   RATANA T., AMORNPITOKSUK P., RATANA T., SUWANBOON S., *The wide band gap of highly oriented nanocrystalline Al doped ZnO thin films from sol–gel dip coating*, J. Alloys Compounds **470**, pp. 408–412, 2009.

[32]   SUN X.W., KWOK H.S., *Optical properties of epitaxially grown zinc oxide films on sapphire by pulsed laser deposition*, J. Appl. Phys. **86**, pp. 408–411, 1999.

[33]   LIN -moh K., TSAI P., *Parametric study on preparation and characterization of ZnO: Al films by sol–gel method for solar cells*, Mat. Sci. Eng. B **139**, pp. 81–87, 2007.

[34]   ASHKENOV N., MBENKUM B.N., BUNDESMANN C., RIEDE V., LORENZ M., SPEMANN D., KAIDASHEV E.M., KASIC A., SCHUBERT M., GRUNDMANN M., WAGNER G., NEUMANN H., DARAKCHIEVA V., ARWIN H., MONEMAR B., *Infrared dielectric functions and phonon modes of high-quality ZnO films*, J. Appl. Phys. **93**, pp. 126–134, 2003.

[35]   BI C., PAN L., XU M., YIN J., GUO Z., QIN L., ZHU H., XIAO J.Q., *Raman spectroscopy of Co-doped wurtzite ZnS nanocrystals*, Chem. Phys. Lett. **481**, pp. 220–223, 2009.

[36]   ALIM K.A., FONOBEROV V.A., SHAMSA M., BALADIN A.A., *Micro-Raman investigation of optical phonons in ZnO nanocrystals*, J. Appl. Phys. **97**, p. 124313, 2005.

[37]   SERNELIUS B.E., BERGGREN K.-F., JIN Z.-C., GRANQVIST C.G., *Band-gap tailoring of ZnO by means of heavy Al doping*, Phys. Rev. **37**, pp. 10244–48, 1988.

[38]   DING J.J., MA S.Y., CHEN H.X., SHI X.F., ZHOU T.T., MAO L.M., *Influence of Al-doping on the structure and optical properties of ZnO films*, Physica B **404**, pp. 2439–2443, 2009.

[39]   ELILARASSI R., CHANDRASEKARAN G., *Effect of annealing on structural and optical properties of zinc oxide films*, Mater. Chem. Phys. **121**, pp. 378–384, 2010.

[40]   PLUGARU R., PLUGARU N., MIHAIU S., VASILE E., *On the electrical conductivity in Al:ZnO layers; experimental investigation and a theoretical approach*, International Semiconductor Conference, Proceedings CAS, pp. 345–348, 2010.

[41]   GOSWAMI N., SHARMA D.K., *Absorption and fluorescence emission in the bulk ZnO and nc ZnO*, Physica E **42**, pp. 1675–1682, 2010.

[42]   PLUGARU R., PLUGARU N., *First Principles Electronic Structure Study of Disordered Al, Ti, Mn Doped ZnO*, Abstract book "Ψk Conference 2010", p. 349. http://www.psi-k.org/conference 2010.

[43]   PLUGARU R., PLUGARU N., *First principles study of the electronic structure of Al/Ti:ZnO Crystal*, International Semiconductor Conference, Proceedings CAS, pp. 383–386. 2009.

[44]   PERDEW J.P., WANG Y., *Accurate and simple analytic representation of the electron-gas correlation energy*, Phys. Rev. B **45**, pp. 13244–13249, 1992.

[45]   VENKATESAN M., FITZGERALD C.B., LUNNEY J.G., COEY J.M.D., *Anisotropic Ferromagnetism in Substituted Zinc Oxide*, Phys. Rev. Lett. **93**, pp. 177206–4, 2004.

[46]   OSUCH K., LOMBARDI E.B., GEBISKI W., *First principles study of ferromagnetism in $Ti_{0.0625} Zn_{0.9375} O$*, Physical Review B, **73**, p. 075202, 2006.

[47]   OHNO H., *Properties of ferromagnetic III-V semiconductors*, J. Magn. Magn. Mat. **200**, () pp. 110–129, 1999.